JOURNAL OF SYNCHROTRON RADIATION
ISSN 1600-5775

The competitive growth of cubic domains in $Ti_{1-x}Al_xN$ films studied by diffraction anomalous near-edge structure spectroscopy

Y. Pinot,[a] M.-H. Tuilier,[a]* M.-J. Pac,[a] C. Rousselot[b] and D. Thiaudière[c]

[a]Université de Haute-Alsace, Laboratoire de Physique et Mécanique Textiles (EA 4365), Equipe Propriétés Physiques et Mécaniques des revêtements, 61 rue Albert Camus, F-68093 Mulhouse, France, [b]Université de Franche-Comté, Franche-Comté Electronique, Mécanique, Thermique et Optique – Sciences et Technologies (UMR CNRS 6174), BP 71427, F-25211 Montbéliard, France, and [c]Synchrotron Soleil, Saint Aubin, F-91192 Gif sur Yvette, France.
*Correspondence e-mail: marie-helene.tuilier@uha.fr

Received 23 April 2015
Accepted 1 September 2015

Edited by S. M. Heald, Argonne National Laboratory, USA

Keywords: diffraction anomalous fine structure; X-ray absorption fine structure; X-ray diffraction; metallic nitride film.

Titanium and aluminium nitride films deposited by magnetron sputtering generally grow as columnar domains made of oriented nanocrystallites with cubic or hexagonal symmetry depending on Al content, which are embedded in more disordered grain boundaries. The substitution of Al atoms for Ti in the cubic lattice of the films improves their resistance to wear and oxidation, allowing their use as protective coatings. Ti *K*-edge X-ray absorption spectroscopy, which probes both crystallized and more disordered grain boundaries, and X-ray diffraction anomalous fine structure, which is sensitive to short- and long-range order within a given crystallized domain, are carried out on a set of $Ti_{1-x}Al_xN$ films deposited by magnetron sputtering on Si substrates. Attention is paid to the shape of the pre-edge region, which is sensitive to the symmetry of the site occupied by Ti atoms, either octahedral in face-centred-cubic Ti-rich (TiN, $Ti_{0.54}Al_{0.46}N$) samples or tetrahedral in hexagonal-close-packed Al-rich ($Ti_{0.32}Al_{0.68}N$) films. In order to obain information on the titanium environment in the well crystallized areas, subtraction of the smooth part of the energy-dependent structure factor for the Bragg reflections is applied to the pre-edge region of the diffraction anomalous data in order to restore their spectroscopic appearance. A flat pre-edge is related to the typical octahedral environment of Ti atoms for cubic reflections. The difference observed between pre-edge spectra associated with face-centred-cubic 200 and 111 Bragg reflections of $Ti_{0.54}Al_{0.46}N$ is assigned to Ti enrichment of 111 large well ordered domains compared with the more disordered 200 ones. The sharp peak observed in the spectrum recorded from the hexagonal 002 peak of $Ti_{0.32}Al_{0.68}N$ can be regarded as a standard for the pure tetrahedral Ti environment in hexagonal-close-packed nitride.

1. Introduction

Nanocrystalline metallic nitride films are currently used as protective coatings to improve lifetime mainly due to their following properties: high hardness, good resistance to abrasive and chemical wear and thermal stability (Musil, 2000). These nitrides are often used under industrial conditions such as high temperature and aggressive environments. TiN is the first generation of hard coatings prepared by physical vapour deposition (PVD) and has been widely used since. However, it shows poor wear resistance at high temperatures due to the formation of a TiO_2 oxide layer with poor tribological properties. The second generation of hard coatings is ternary thin films like $Ti_{1-x}Al_xN$ with improved hardness and Young's modulus and better oxidation resistance (Hakansson *et al.*, 1987; Adibi *et al.*, 1991; Padley & Deevi, 2003). $Ti_{1-x}Al_xN$ films can be considered as a model system, where TiN crystallizes in

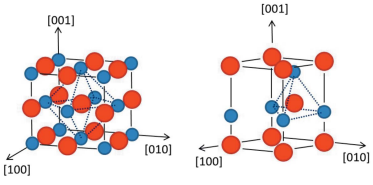

a face-centred cubic (f.c.c.) lattice and AlN in a hexagonal close packed (h.c.p.) wurtzite-type lattice. The best mechanical properties are obtained for the maximum Al content substituted for Ti in the f.c.c. lattice (Hugosson *et al.*, 2003). Early transmission electron microscopy (TEM) studies of Ti-rich films have shown that the films present a columnar microstructure and the limited solubility of AlN in TiN has the effect of precipitating h.c.p. nanograins outside of the f.c.c. crystallized columns (Adibi *et al.*, 1991; Wahlström *et al.*, 1993). TEM analysis of $Ti_{1-x}Al_xN$ films as a function of x have shown f.c.c. single-phase coatings at low Al content and dual-phase or h.c.p. coatings at higher Al content (Mayrhofer *et al.*, 2003; Kutschej *et al.*, 2005; Hörling *et al.*, 2005). Hardening from the formation of a coherent nanocomposite structure by spinodal decomposition has been highlighted in metastable $Ti_{1-x}Al_xN$ films (Rachbauer *et al.*, 2011; Schalk *et al.*, 2012). The proportion of grain boundaries plays a major role on the ductile property and resistance to wear. The role of the low miscibility on the proportion of grain boundaries is not well understood. A promising way to explore the nanostructure of the films consists of systematically probing the elements present in order to detect their localization either in the crystallized part or in grain boundaries.

It is well known that the mechanical performances of hard coatings with columnar microstructure are related to the ability of well oriented columns to slide against each other through grain boundaries made of poorly crystallized or amorphous domains. X-ray diffraction (XRD) gives the lattice symmetry of crystallized domains, but is unable to take into account the less crystallized area present in grain boundaries. In such complex materials, other probes like core-level spectroscopies are of a great interest for a thorough investigation of the structure at micrometre and nanometre scales. X-ray absorption fine structure (XAFS) is a powerful tool for providing insight into the electronic structure and local environment of atoms present in complex materials like metallic nitrides films. It has allowed a separate structural investigation of metallic components of multilayer systems (Ersen *et al.*, 2003, 2005; Tavares *et al.*, 2004). The evolution of Al and Ti *K*-edges (1550 eV, 4968 eV) spectra in the $Ti_{1-x}Al_xN$ system has been reported (Tuilier *et al.*, 2007, 2008; Gago *et al.*, 2009). The Al and Ti coordination is either tetrahedral or octahedral and determines the shape of their X-ray absorption near-edge structure (XANES). The local environment of Ti or Al atoms in nitrides is shown schematically in Fig. 1. In the centrosymmetric cubic B1 NaCl lattice type, six nitrogen atoms at $R_c = a_c/2$ surround Ti atoms. In the non-centrosymmetric hexagonal (wurtzite-type) lattice, the atoms occupy the centre of a slightly distorted tetrahedron, and the nearest-neighbour distance is the weighted average of $R_{h1} = 3c_h/8$ and $R_{h2} = [(a_h/3)^2 + (c_h/64)^2]^{1/2}$. These coordination radii are quite different, around 2.1 and 1.9 for R_c and R_h, respectively. The coexistence of cubic and hexagonal Ti environments in the same sample has been emphasized by XAFS analysis of $Ti_{0.32}Al_{0.68}N$ thin film (Tuilier *et al.*, 2008). The XAFS technique presents indeed the drawback to probing both crystalline and non-crystalline domains. By combining the selectivity

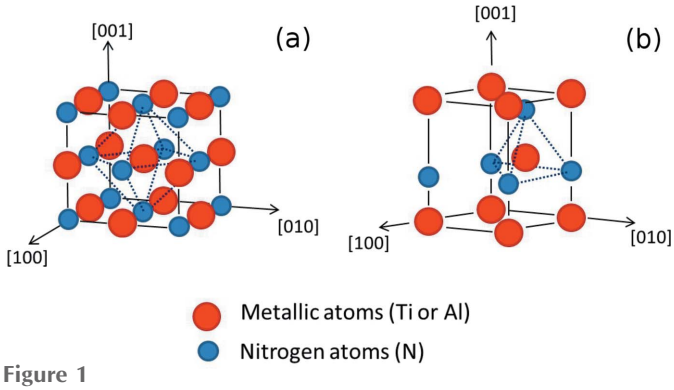

Figure 1
Scheme of the (*a*) face-centered cubic (f.c.c.) lattice with octahedral site, (*b*) hexagonal lattice (h.c.p.) with tetrahedral site.

on the lattice symmetry of XRD and the local approach of XAFS, diffraction anomalous fine-structure spectroscopy (DAFS) allows a separate investigation of crystalline domains regardless of poorly crystallized area. It has been extensively used to solve separately the local atomic structure around non-equivalent crystallographic sites in crystallized and epitaxial grown materials (Cross *et al.*, 1998; Proietti *et al.*, 1999).

In the present work, the XAFS and DAFS spectra recorded from a set of Ti-rich (TiN, $Ti_{0.54}Al_{0.46}N$) and Al-rich ($Ti_{0.32}Al_{0.68}N$) metallic nitride films deposited by radio-frequency (RF) magnetron sputtering are presented. In such complex materials, which present a competitive growth of domains with various orientations, an accurate normalization of DAFS data is difficult to carry out, as standard spectra recorded from (Ti, Al)N single crystals are obviously unavailable. Kawaguchi *et al.* (2014) have recently revisited the analysis of diffraction anomalous near-edge structure (DANES) spectra recorded on powder materials. That work points out the difficulty of fitting the DANES data because the number of fitting parameters generally exceeds the number of experimental data points. Fortunately, in the case of titanium nitrides, the pre-edge region provides rich information on the symmetry of the sites occupied by Ti atoms in nano-crystalline areas. The data reduction carried out in the present work consists of a subtraction of the smooth part of the energy-dependent structure factor for the Bragg reflections in order to provide valuable information on the short-range order in crystallized domains.

2. Experimental details

2.1. Sample elaboration

$Ti_{1-x}Al_xN$ coatings were deposited onto a Si (100) wafer at room temperature by RF magnetron reactive sputtering of a metallic target in ArN_2 plasma. The thickness of the films was adjusted to be between 1.9 and 2.1 µm to within 0.05 µm. The deposition parameters were chosen in order to operate in reactive mode, allowing a stoichiometric nitrogen composition in the film. Two types of deposits were carried out in the present work: (i) from mosaic targets made of metallic tita-

nium (99.6%) and aluminium (99.9%); (ii) from TiAl sintered targets produced by powder metallurgy. Thin metallic $Ti_{1-x}Al_x$ interlayers of thickness 45 nm have been deposited before the $Ti_{1-x}Al_xN$ coatings for enhancing adhesion. More details of the elaboration process and targets used are described in earlier work (Pinot *et al.*, 2015).

2.2. Characterization method

Energy-dispersive X-ray emission spectroscopy was used to determine the film composition using a scanning electron microscope (Jeol JSM-56000Lv). Film thicknesses were measured by the step method using a mechanical profilometer.

The DAFS and XAFS experiments were performed at the DIFFABS beamline of the French synchrotron SOLEIL. In our case SOLEIL was running at 2.75 GeV with an average current of 430 mA, in the TOP/UP configuration (continuous refill). The monochromatization and horizontal focusing were achieved using a fixed-exit double Si (111) crystal monochromator. Two long cylindrical mirrors (50 nm Rh deposited on Si substrates) located in front of and behind the monochromator were optimized for good efficiency of harmonic rejection. The first one is located between the source and the monochromator and allows the vertical beam to be collimated in order to increase the energy resolution. The second one focuses the monochromatic X-ray beam along the vertical direction. For these experiments the angle of incidence of both mirrors was 6 mrad. In that configuration the spot size at the sample position was 300 µm × 330 µm [vertical and horizontal full width at half-maximum (FWHM)]. The main instrument in the experimental hutch is a six-circle diffractometer, equipment built for the synchrotron facility. Four circles allow sample orientation and the other two circles are dedicated to X-ray diffraction measurements in the vertical and horizontal planes. For these experiments the maximum intensities of the 111c, 200c and 002h Bragg peaks of nitride films were recorded in the Ti *K*-edge region (4900–5600 eV) by using a Vortex-EX® silicon drift detector (SDD) located on the detector arm, just behind the detection slits. The DAFS spectra were recorded in a top-DAFS scan mode. The detection of fluorescence emission was performed using another SDD, a Vortex-ME4® model. The self-absorption effect, which causes distortions of spectra due to a change in the mean absorption depth as a function of the incident photon energy, was corrected by the Booth algorithm using *Athena* software (Ravel & Newville, 2005). Moreover, the Lorentz-polarization correction was also taken into account in the experimental spectra.

3. Results and data analysis

3.1. X-ray diffraction profiles

Typical X-ray diffraction profiles recorded at E = 4900 eV for TiN and $Ti_{0.54}Al_{0.46}N$ 200, $Ti_{0.54}Al_{0.46}N$ 111 and $Ti_{0.32}Al_{0.68}N$ 002 Bragg peaks are presented in Fig. 2(*a*). For $Ti_{0.54}Al_{0.46}N$, the 200 peak is shifted towards the high angles compared with that of TiN indicating a decrease in the mean lattice parameter due to incorporation of Al atoms. The 200 lattice parameters are found to be 4.29 ± 0.02 Å and 4.23 ± 0.01 Å for TiN and $Ti_{0.54}Al_{0.46}N$, respectively. For the latter, the lattice parameter is slightly smaller (4.21 ± 0.01 Å) for the 111 reflection than for the 200 reflection. For $Ti_{0.54}Al_{0.46}N$ film, the 200 lattice parameter is found to be 4.23 Å, instead of 4.18 Å for an ideal stress-free $Ti_{0.54}Al_{0.46}N$ solid solution following Vegard's law. The higher value of the lattice parameter than expected for that composition seems to be consistent with previous TEM analyses, which have shown an enrichment of AlN nanograins outside the columns (Adibi *et al.*, 1991, 1993). For $Ti_{0.32}Al_{0.68}N$, the 002 hexagonal lattice parameter is 5.08 ± 0.01 Å. This value is higher than for AlN due to the incorporation of Ti atoms. The FWHM of the 200 peak shows a reduction by a factor of two in cubic $Ti_{0.54}Al_{0.46}N$ with respect to TiN film. The FWHM value of the 111 peak is twice a small as the 200 peak in $Ti_{0.54}Al_{0.46}N$ indicating a high texturation along the [111] direction. The narrower rocking curve of the 002 peak of $Ti_{0.32}Al_{0.68}N$ is explained by the well oriented fibrillar texture observed in Al-rich films (Tuilier *et al.*, 2012). Two factors influence the FWHM: the length of the grains within the columns and the orientation of the grains with respect to each other. For distorted hetero-epitaxial layers the coherence length is defined as the average extension of the crystal lattice regions, which scatters coherently. The film is assumed to consist of mosaic blocks with mean vertical and lateral dimensions. For PVD-deposited films with columnar microstructure, the FWHM values of the XRD peaks have to be considered with caution. Although the structural information is more qualitative in this

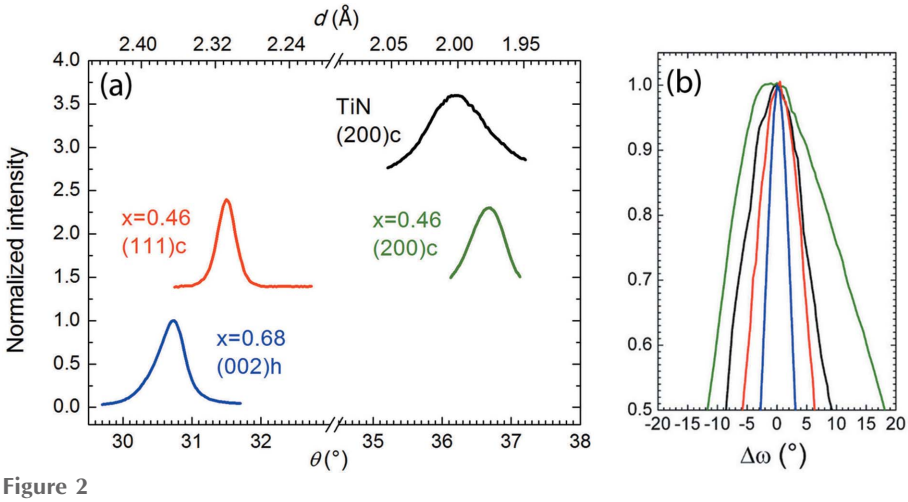

Figure 2
(*a*) X-ray diffraction peaks of $Ti_{1-x}Al_xN$ films recorded at 4900 eV and (*b*) their corresponding rocking curves.

case than for heteroepitaxial films, it is very useful for understanding the relation between microstructure and nanostructure. Thereby, it is possible to define the coherence length along the growth direction with Scherrer's formula. The coherence length varies from 167 Å for TiN to almost 300 Å for $Ti_{0.32}Al_{0.68}N$ film (Tuilier *et al.*, 2012). For $Ti_{0.54}Al_{0.46}N$, a significant difference in the coherence length value is observed between 111 and 200 cubic domains, 258 Å and 140 Å, respectively. Those values are obviously five to ten times lower than for epitaxically grown metallic nitride layers of rock salt structure (Willmann *et al.*, 2008).

Fig. 2(*b*) shows the rocking curves for the various reflections, which involve both lateral coherence length and mosaicity of the domains. The FWHM of the 200 rocking curve is much higher for TiN (29.0 ± 1.5°) than for $Ti_{0.54}Al_{0.46}N$ (18 ± 1°), indicating a better texture. Indeed, these values are significantly higher than those of epitaxial layers, of about one order of magnitude. The 111 rocking curve of $Ti_{0.54}Al_{0.46}N$ is even narrower (13 ± 1°). Thus XRD analysis provides an evaluation of the size of the nanocrystallites for the interpretation of spectroscopic data in terms of cluster-size dependence.

3.2. X-ray absorption and diffraction anomalous spectra

The raw Ti *K*-edge XANES and DANES spectra of the TiN, $Ti_{0.54}Al_{0.46}N$ and $Ti_{0.32}Al_{0.68}N$ samples are presented in Fig. 3. Ti *K*-edge XANES spectra provide information on the electronic and atomic structure of the films. The main structural information comes from the pre-edge region. There is a striking similarity between the Ti *K* pre-edge peaks of Ti oxides and nitrides. Farges *et al.* (1997) have studied a set of model compounds where Ti has various coordinations and pointed out the location of Ti pre-edge features about 18 eV before the main XANES crest. The difference in energy between the main peak and the pre-edge features of Ti nitrides is quite similar, about 16 eV. These pre-edge features are assigned to the electronic transitions dipole-forbidden 1*s*–3*d* transition. Due to the mixing of the 3*d* states with the *p* orbitals of the ligand, the transition becomes partially allowed depending on the symmetry of the metallic site. In the equivalent molecular orbital or ligand field description of this feature, mixing of *d* and *p* orbitals is possible when the absorbing atom is not a centre of symmetry, thus allowing this dipole transition. Therefore, the Ti 3*d*–N 2*p* mixing is much stronger when the Ti absorbing atoms are at the centre of a tetrahedron than of an octahedron. The greatest impact on the pre-edge peak arises from a reduction in Ti–ligand bond length (Jiang *et al.*, 2007). In agreement with that assessment and previous studies of oxide materials, the pre-edge features of ternary nitrides XANES are found to have the greatest height for fourfold-coordinated Ti atoms. Fig. 3(*a*) shows the evolution of the intensity and position of the pre-edge peaks according to the *x* content of $Ti_{1-x}Al_xN$ films. The pre-edge peaks of TiN and $Ti_{0.54}Al_{0.46}N$ are at 4971.5 eV and at 4971.0 eV, respectively. The sharp pre-edge peak at 4969.4 eV in $Ti_{0.32}Al_{0.68}N$ XANES proves that a large part of the Ti atoms are incorporated in the tetrahedral sites of hexagonal AlN-type columns (Tuilier *et al.*, 2008). As for model Ti oxides, the pre-edge observed in the DANES spectrum of cubic $Ti_{0.54}Al_{0.46}N$ is quite smooth and shifted to higher energy by about 2 eV compared with the former.

The raw Ti *K*-edge DANES spectra related to peaks of significant intensities in XRD spectra of TiN, $Ti_{0.54}Al_{0.46}N$ and $Ti_{0.32}Al_{0.68}N$ are shown in Fig. 3(*b*). Below 4973 eV, the DANES data of cubic materials (TiN and $Ti_{0.54}Al_{0.46}N$) look quite similar with a flat pre-edge between 4968 and 4971 eV. The pre-edge peak recorded at the 002 Bragg peak of $Ti_{0.32}Al_{0.68}N$ is well defined and has its maximum at 4969 eV as expected for fourfold-coordinated Ti atoms. Some difference in the DANES and XANES pre-edge regions are difficult to appreciate in the raw data, so a suitable background subtraction described above is required for an easier comparison. Beyond 4974 eV, the shape of the DANES spectra related to cubic reflections is significantly different. $Ti_{0.54}Al_{0.46}N$ DANES data recorded on the 111 peak resembles TiN (200). Both have a sharp minimum at 4974 eV, while spectra of $Ti_{0.54}Al_{0.46}N$ (200) and $Ti_{0.32}Al_{0.68}N$ (002) look almost similar with a shoulder at 4974 eV and a smooth peak around 4983 eV.

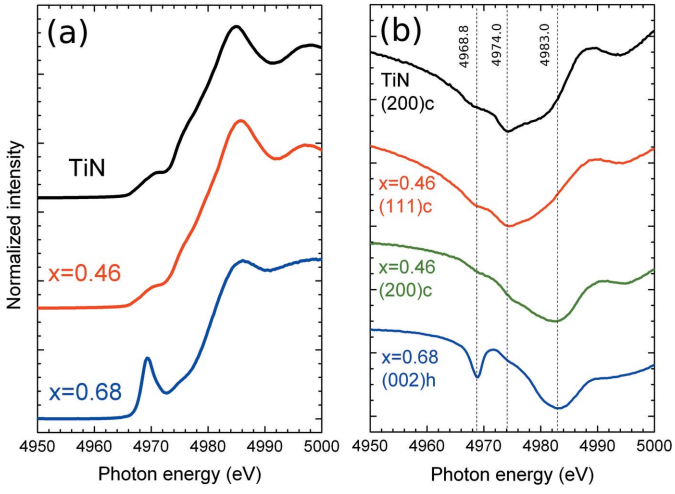

Figure 3
Ti *K*-edge (*a*) XANES and (*b*) DANES raw spectra of $Ti_{1-x}Al_xN$ films.

3.3. XANES modelling of the pre-edge region

XANES spectra were calculated using the *ab initio* full multiple-scattering code *FEFF9* (Rehr *et al.*, 2009; Jorissen & Rehr, 2010). This approach is based on a hybrid scheme incorporating a reciprocal-space calculation of the multiple-scattering equations, together with a real-space calculation of the excitation spectrum. It uses the extended continuum approximation to treat all XANES features in terms of the scattering of continuum photoelectrons, including those usually ascribed to bound electronic transitions. Farges *et al.* (1997) used that approach in modelling the pre-edge region of titanium oxides. To our knowledge, FEFF calculations have

not been performed on the pre-edge region of titanium nitrides so far.

The XANES calculations by *FEFF9* were carried out on cubic and hexagonal-like Ti environments with a cluster of about 100 atoms for both. A Ti atom was defined as the absorbing atom located at the centre of a cluster in the tetrahedral and octahedral site for hexagonal and cubic lattices, respectively. For cubic environment modelling, the cluster was built with Ti and N atoms around the absorbing atom, with a lattice constant (f.c.c.) of a = 4.2420 Å. With regard to XANES modelling on the hexagonal environment, the cluster was built with Al and N atoms around the Ti absorbing atom, with a lattice constant (h.c.p.) of a = 3.1114 Å and c = 4.9792 Å. The lattice distortion by the Ti atom in the AlN (h.c.p.) system has not been taken into account. The muffin-tin radii were chosen for TiN (f.c.c.) and AlN (h.c.p.) as 1.3 and 1.15, respectively. The self-consistent field (SCF) calculations were performed on a cluster of 20 atoms. The full multiple scattering (FMS) (Ankudinov *et al.*, 1997) was performed on a cluster of 100 atoms around the absorbing atom and the exchange potential was of the Hedin–Lundqvist type, which is recommended for solids. The correlated Debye model has been used to calculate Debye–Waller factors for each path of the TiN (f.c.c.) modelling at a temperature of 300 K. The energy positions of the Ti K pre-edge peaks were adjusted onto the experimental spectra.

Details of the pre-edge XANES spectra modelling are represented in Fig. 4. The fourfold coordination of Ti atoms embedded in the h.c.p. lattice gives rise to a sharp pre-edge peak, whereas a step is observed for the sixfold coordination in rock-salt TiN. The modelling of the Ti K pre-edge region is in good agreement with experimental results in Fig. 3.

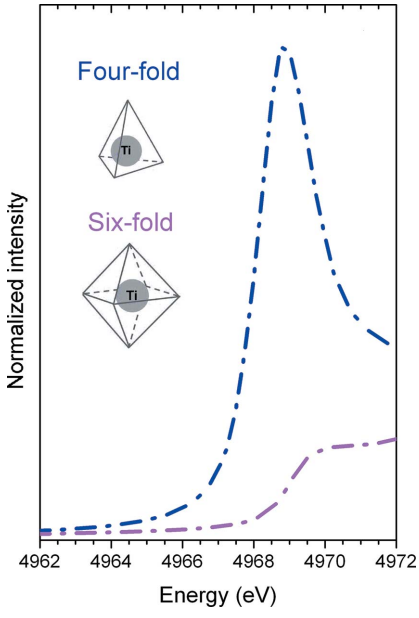

Figure 4
Modelling of Ti K pre-edge region for Ti-rich and Al-rich films using *FEFF9*.

3.4. DANES data treatment

Raw DANES data of TiN, $Ti_{0.54}Al_{0.46}N$ and $Ti_{0.32}Al_{0.68}N$ films recorded at the Ti K-edge are presented together with XANES spectra in Fig. 3(b). First, absorption corrections were performed on the experimental DANES spectra in order to take into account the absorption $A(E)$ of X-rays within the film as a function of photon energy. The diffracted intensity is

$$I(Q, E) \propto |F(Q, E)|^2 A(E) LP. \quad (1)$$

The Lorenz (L) and polarization (P) corrections vary slowly with photon energy instead of absorption. For $Ti_{1-x}Al_xN$ thin films the absorption coefficient μ is proportional to the scattering factors f'' (see above) divided by the atomic mass of each element contained in the film (Hodeau *et al.*, 2001),

$$\mu \propto \frac{(1-x) f''_{Ti} + x f''_{Al} + f''_{N}}{(1-x)M_{Ti} + xM_{Al} + M_{N}}. \quad (2)$$

The XANES (green lines), raw DANES (blue lines) and corrected DANES (pink lines) spectra are drawn in Fig. 5. The imaginary part of the Ti scattering factor was extracted from the XANES fluorescence spectra, including the pre-edge region.

The absorption correction has no significant effect on the position of the structures in the pre-edge region, up to 4974 eV. However, it is difficult to compare the pre-edge fine structures (PEFS) because of the shape of the diffracted continuous background. The aim of the tentative data treatment presented below is to give to the pre-edge region of the DANES data a shape as close as possible to the XANES data in order to extract the information on the local order in the crystallized domains regardless of grain boundaries. That point of view is quite different from the usual analyses of DANES (Alamagna *et al.*, 1998).

In DAFS experimental conditions, the diffracted intensity is proportional to the square modulus of the unit-cell structure factor,

$$I(Q, E) \propto |F(Q, E)|^2. \quad (3)$$

The unit-cell factor structure is defined as

$$F(Q, E) = \sum_j f_j(E) \exp\left(iQ.r_j\right). \quad (4)$$

f_j and $\mathbf{r}_j$ are the scattering factor and the distance vector of the jth atom in the unit cell, Q is the scattering vector and E the energy of the incident beam. The complex atomic scattering factor f of the atom j may be split into a smooth part and an oscillatory part

$$f_j(E) = f^0 + f'(E) + if''(E) + \Delta f''(E)[\chi'(E) + i\chi''(E)]. \quad (5)$$

The three first terms are the Thomson scattering (f^0) and anomalous corrections to f^0 at the absorption-edge energy (f' and f''). The last term is the correction to the scattering factor due to the local environment of the anomalous atom above the edge. It contains $\Delta f''$, which is similar to a step edge, and $\chi''(E)$ and formally identical to XAFS in absorption spectra (Stragier *et al.*, 1992). As the present work focuses on the pre-

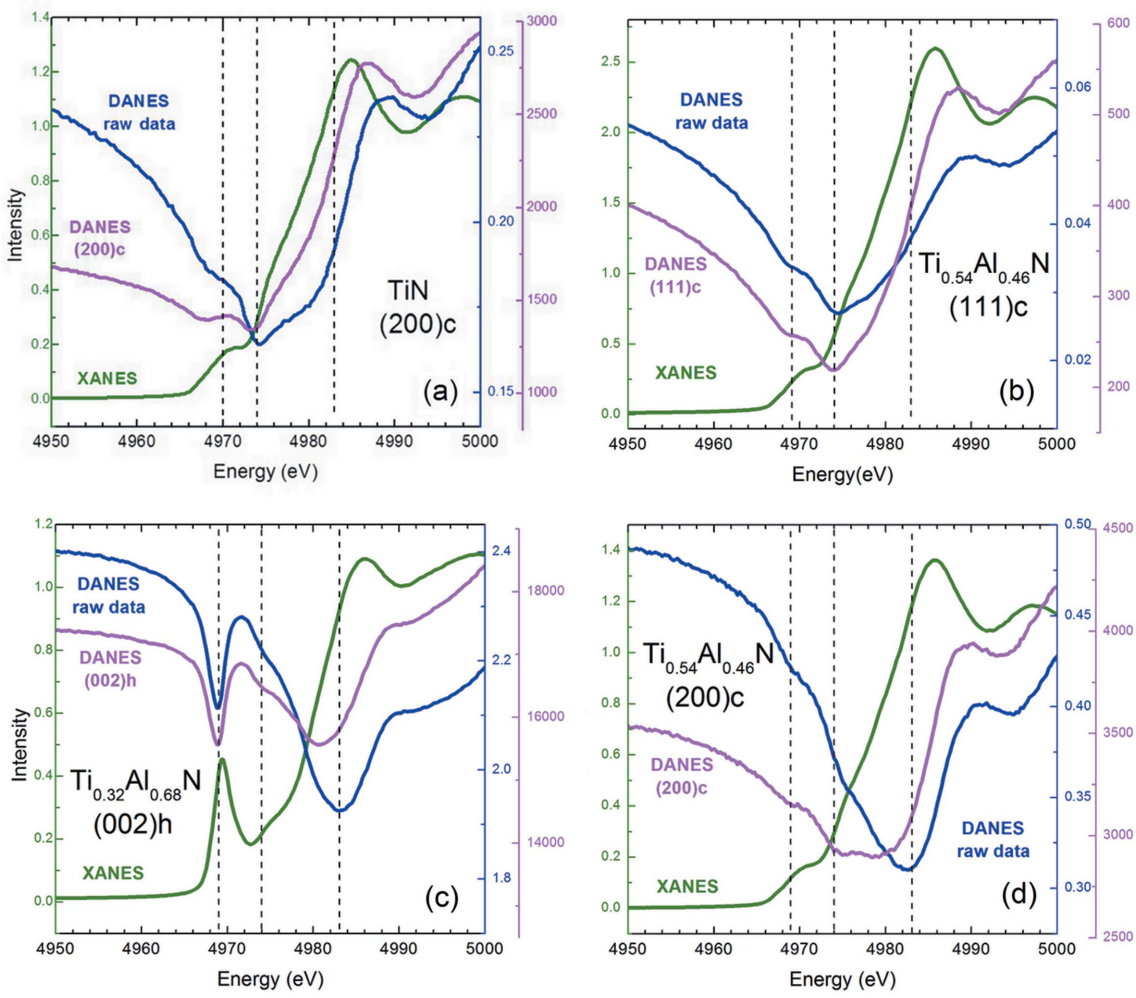

Figure 5
Raw and corrected Ti *K*-edge DANES and XANES spectra: (*a*) 200c reflection of TiN, (*b*) 111c reflection of $Ti_{0.54}Al_{0.46}N$, (*c*) 002h reflection of $Ti_{0.32}Al_{0.68}N$, (*d*) 200c reflection of $Ti_{0.54}Al_{0.46}N$.

edge fine-structure (PEFS) region, below the absorption edge, $\Delta f''$ vanishes and the last term is not to be considered.

Fitting DANES data has been previously used to obtain both site occupancy and site-specific valences because it is sensitive to a specific crystallographic site in a phase (*e.g.* it can be used to investigate the tetrahedral and the octahedral site of spinels). With f'' being proportional to the absorption coefficient μ, the way to fit the anomalous DRX data was to extract the fine structure of f'' from the XANES measurement of a standard sample and then to use the Kramers–Kronig relation to obtain the energy-dependent f' anomalous factor containing the DANES. f' can indeed be calculated through the Kramers–Kronig relation if f'' is known, and *vice versa*.

The anomalous factors (f' and f'') were calculated using the *DELTAF* routine of the *DIFFKK* program (Cromer & Liberman, 1981; Cross *et al.*, 1998). The natural width of the *K* level of Ti (~1.2 eV) was taken into account in computing of anomalous factors.

For complex samples made of crystallized domains embedded in grain boundaries, knowledge of the local order of elements within the ordered lattice regardless of more disordered environments is of crucial importance. The fitting technique described below is therefore not well suited to ternary $Ti_{1-x}Al_xN$ nitrides because XANES spectra of standard samples containing metallic elements in pure tetrahedral or octahedral environments are not available. In that case, it seems more useful to extract experimental DANES from the measured data using an appropriate background subtraction allowing a comparison with XANES data of a given sample. In order to reduce DANES to a XANES-like spectrum, we have to calculate the smooth part of the energy-dependent structure factor for the Bragg reflections under consideration.

For the cubic $Ti_{1-x}Al_xN$ 200 reflection,

$$F_{200} = 4(1-x)\left[f^0_{\rm Ti} + f'_{\rm Ti}(E) + if''_{\rm Ti}(E)\right] + 4xf^0_{\rm Al} + 4f^0_{\rm N}. \quad (6)$$

For the cubic $Ti_{1-x}Al_xN$ 111 reflection,

$$F_{111} = 4f^0_{\rm N} - 4(1-x)\left[f^0_{\rm Ti} + f'_{\rm Ti}(E) + if''_{\rm Ti}(E)\right] - 4xf^0_{\rm Al}. \quad (7)$$

For the hexagonal $Ti_{1-x}Al_xN$ 002 reflection,

$$F_{002} = 2(1-x)\left[f^0_{\rm Ti} + f'_{\rm Ti}(E) + if''_{\rm Ti}(E)\right] + 2xf^0_{\rm Al} + 2if^0_{\rm N}. \quad (8)$$

The calculated square modulus of structure factors F_{hkl} of each reflection are presented as a function of the photon energy in Fig. 6. The shape of the curves governs the smooth back-

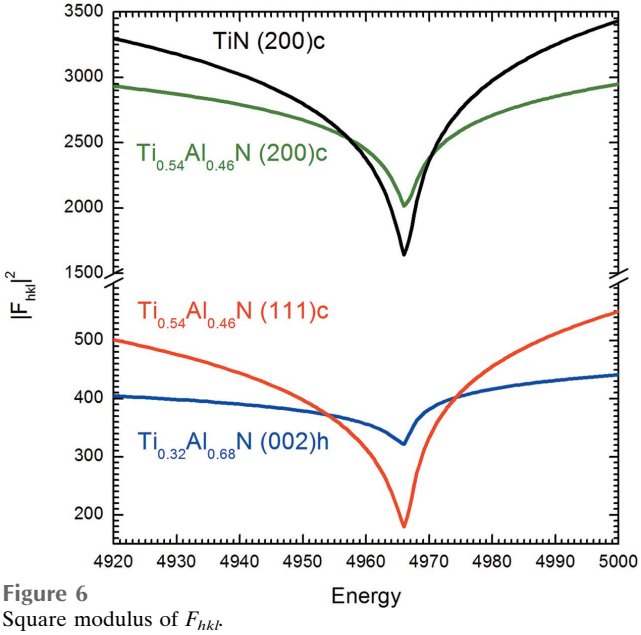

Figure 6
Square modulus of F_{hkl}.

ground of the diffracted intensity. The contribution of f' and f'' differ depending on the reflections. The f' contribution prevails for the 111 and 200 cubic reflections while the f'' contribution is significant for the hexagonal 002 reflection.

The smooth background intensity was adjusted to the background of the experimental DANES spectra below the Ti *K*-edge and then subtracted (Fig. 7*a*). In this way, although an uncertainty remains on the true intensity of the features, a comparison with XANES spectra (Fig. 7*b*) becomes possible. Beyond the pre-edge region, an inflection point is present around 4974 eV in all DANES spectra that is well emphasized by the data treatment. The minimum of f' (Ti *K*-edge threshold value) was adjusted to 4974 eV for the subtraction of the contribution of diffraction. That change in the slope, which occurs at the same value as in the XANES spectra, is assigned to transitions from 1*s* towards *np* Rydberg-like states.

Fig. 8 shows the pre-edge region of the DANES spectra after background subtractions. The shape of the pre-edge fine structure (PEFS) is enhanced by the background subtraction. Pre-edge peaks recorded from cubic reflections present a smoothed pre-edge extending from 4969 to 4972 eV, which looks more marked in DANES than in XANES. In contrast, the intense and symmetrical pre-edge peak recorded from the hexagonal reflection of $Ti_{0.32}Al_{0.68}N$ is typical of Ti regular tetrahedral coordination.

4. Discussion

As the growth orientation of f.c.c. TiN and low Al content films is along the [200] direction, the $Ti_{0.54}Al_{0.46}N$ sample includes additional grains oriented along [111], which grow larger than the former. Indeed, the comparison between the 200 and 111 peak profiles of $Ti_{0.54}Al_{0.46}N$ (Fig. 2) shows that the size and lateral coherency of the 111 grains are much better than those of the 200 profiles. Earlier works have reported such behaviour (Adibi *et al.*, 1993; Beckers *et al.*, 2005). On these points, our results are in fair agreement with the work of Beckers *et al.* (2005). However, these authors have assigned such difference in growth to an enrichment of 111 grains in Al atoms with respect to the 200 ones. Indeed, the

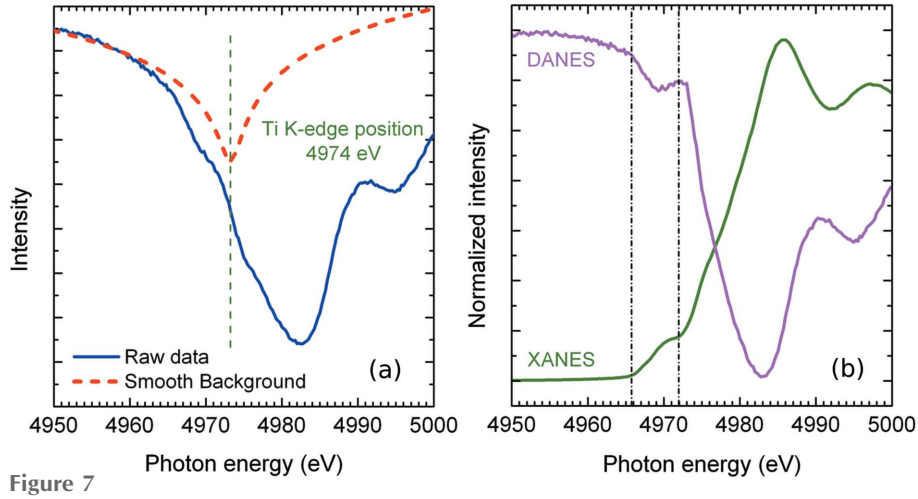

Figure 7
(*a*) Position of the smooth background on raw data before subtraction. (*b*) DANES and XANES spectra normalized.

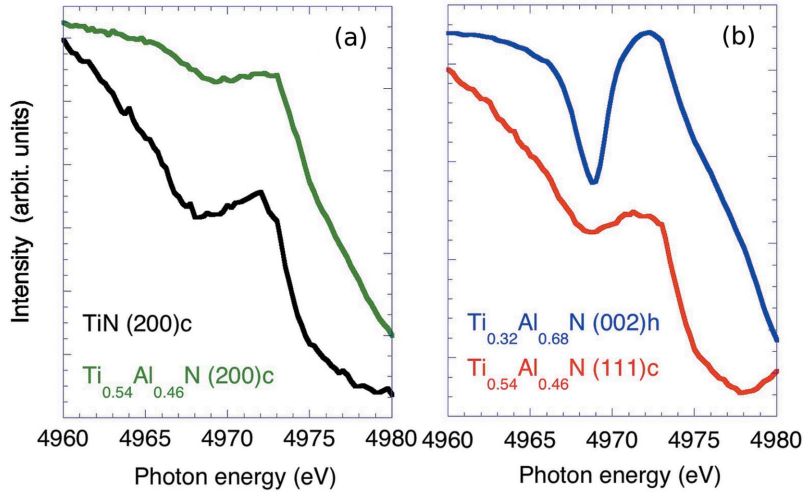

Figure 8
Pre-edge DANES fine-structure spectra after subtraction of the smooth contribution of the diffracted intensity.

$Ti_{0.54}Al_{0.46}N$ lattice parameter derived from the 111 reflection is slightly smaller than that extracted from the 200 one (see above). Considering the Al and Ti atomic radii, this suggests that more Al atoms are incorporated within domains oriented along the [111] direction. As a matter of fact, the situation is probably more complex. Indeed, diffraction anomalous experiments reveal that the Ti *K* DANES spectrum related to the 200 and 111 reflections of $Ti_{0.54}Al_{0.46}N$ look quite different (Fig. 3). In contrast, $Ti_{0.54}Al_{0.46}N$ (111) resembles TiN (200) DANES suggesting that more Ti atoms are incorporated in domains growing along the [111] direction than along the [200] one. XRD parameters are related to long-range order; moreover, diffraction anomalous spectra refer to short-range order around resonant atoms located in the crystallized domains. Therefore, the apparent discrepancy regarding parameter values derived from the 111 and 200 reflections cannot be considered as proof that more Al atoms are incorporated in the former than in the latter domains. In fact, the 200 peak is significantly larger than the 111 peak (Fig. 1), suggesting that the unit cells could undergo substantial distortion along the [200] growth direction. Furthermore, the 200 rocking curve spreads over more than 30° instead of about 10° for the 111 one. This indicates a loss of lateral coherency and a misorientation of the grains with respect to the [200] growth direction. Under these conditions the application of Vegard's law does not make sense.

The features called pre-edge fine structures (PEFS) in transition metals are caused by transitions of the 1*s* electron to the unoccupied electron states near the conduction band originated from Ti 3*d* atomic orbitals, which are forbidden by the dipole selection rules. The mechanism responsible for PEFS formation in perovskite oxides has been thoroughly investigated in previous theoretical and experimental works (Vedrinskii *et al.*, 1998; Woicik *et al.*, 2007). As mentioned below, such studies performed on oxide materials help to understand the origin of the spread of Ti *K*-edge PEFS in Ti cubic nitrides. The 3*d* electronic states form two sets of conduction bands in perovskites, lower t_{2g} bands and upper e_g ones. Calculations performed by the full multiple scattering method (Vedrinskii *et al.*, 1998) have demonstrated that the core hole potential strongly influences both t_{2g} and e_g states. According to these results, PEFS originate several contributions: a weak one, on the low-energy side, is mainly caused by quadrupole transitions of Ti 1*s* electrons to the 3*d* unoccupied t_{2g} type states; they could be the cause of the tail observed from about 4966 to 4970 eV on the low-energy side of cubic nitride pre-edges (Fig. 3). A second peak located at about 3 eV above is assigned to the Ti 1*s* electron transitions resulting from the overlap of Ti 3*d*-derived orbitals e_g and the ligand *p* orbitals. The intensity of the peak strongly depends of the symmetry. The *p*–*d* mixture effect takes place owing to the static and/or dynamic violation of the inversion symmetry relative to the absorbing atom (Vedrinskii *et al.*, 1998). For example, in $SrTiO_3$ perovskite oxide, the PEFS region shows two well identified peaks with a marked splitting of about 2.2 eV (Woicik *et al.*, 2007). The electronic states are more localized in perovskite oxides than in nitrides which explains why a plateau is observed in cubic nitride spectra instead of well identified peaks.

When the symmetry of TiO_6 is reduced from the O_h point group to D_{4h} and furthermore in the C_{4v} non-centrosymmetric point group, in the $SrTiO_3$ thin film or bulk $PbTiO_4$ tetragonal phase, the intensity of the pre-edge peak strongly increases. In h.c.p. nitrides, Ti atoms occupy a slightly distorted tetrahedral site, without inversion symmetry. The well defined pre-edge line in the DANES spectrum recorded at the hexagonal 002 peak of $Ti_{0.32}Al_{0.68}N$ can be regarded as a standard for the pure tetrahedral Ti environment in h.c.p. nitride. Its minimum peaks at 4969 eV, which is approximately the energy of the outset of the plateau of cubic samples' spectra. It can be assigned to the transition of 1*s* electrons to the the e_g states, which are now lower in energy than the t_{2g} ones. The pre-edge peak is more asymmetric in XANES than in DANES, due to the contribution of some sixfold-coordinated Ti atoms out of the crystallized domains to the absorbed intensity on the high-energy side of the peak (Tuilier *et al.*, 2012).

As stated above, a sharp minimum is observed at 4974 eV for TiN (200) and $Ti_{0.54}Al_{0.46}N$ (111) DANES data instead of a shoulder in $Ti_{0.54}Al_{0.46}N$ (200) and $Ti_{0.32}Al_{0.68}N$ (002) spectra (Fig. 6). The main peak of TiN (200) and $Ti_{0.54}Al_{0.46}N$ (111) is broadened with respect to $Ti_{0.54}Al_{0.46}N$ (200) owing to a more prominent contribution around 4974 eV. If we consider XANES results on oxide compounds, the cubic $SrTiO_3$ spectrum shows a more intense peak around 4974 eV than tetragonal $PbTiO_3$. The reduction of 1*s*–4*p* intensity in the latter is assigned to 3*d*–4*p* hybridization, which is allowed in C_{4v} symmetry. The DANES PEFS regions of nitrides (Fig. 8) are more easily comparable with XANES spectra. All DANES spectra present a shoulder at 4974 eV assigned to the 1*s*–4*p* electronic transition. The presence of regular TiN_6 octahedra could have the effect of an enhancement of the 1*s*–4*p* intensity in the $Ti_{0.54}Al_{0.46}N$ (111) DANES region around 4974 eV. The more extended $Ti_{0.54}Al_{0.46}N$ (111) domains present a better long-range order than the (200) ones. In such a well ordered lattice with few distortions, the number of Ti atoms probably outweighs that of Al atoms. It can be noticed that the 111 Ti-enriched domains occupy a small volume compared with the more disordered 200 ones in the $Ti_{0.54}Al_{0.46}N$ sample. The excess of Ti atoms in the (111) areas could be cancelled by nanograins of h.c.p. AlN and/or (TiAl)N that have been identified in earlier work (Adibi *et al.*, 1991; Wahlström *et al.*, 1993).

5. Summary and conclusion

In this work the Ti *K*-edge XANES and DANES spectra recorded on the 200, 111 cubic and 002 hexagonal XRD peaks of $Ti_{1-x}Al_xN$ thin films deposited by RF magnetron sputtering on Si (100) are compared. Such films present a columnar growth with several orientations of nanocrystalline domains embedded in more disordered grain boundaries. The main growth direction of TiN is along the [100] orientation normal to the substrate surface, but as increasing the Al content, the growth of domains oriented along the [111] direction of cubic

lattice takes place. It is well known that the best resistance to wear and oxidation is obtained for the maximum of Al atoms substituted for Ti ones in the cubic lattice. Beyond $x = 0.6$, the crystallized part of the film consists of larger domains, which present the hexagonal lattice symmetry and the layers become brittle and not well suited to their use as protective coatings. For compositions close to the transition such as $Ti_{0.32}Al_{0.68}N$, a co-existence of h.c.p. domains grown along the [002] direction and poorly crystallized f.c.c. 111 nanograins has been shown.

The use of diffraction anomalous fine structure allows investigation of the local order around Ti atoms in nanocrystalline domains regardless of the poorly crystallized areas in grain boundaries. The DANES data recorded from 200 and 111 domains of $Ti_{0.54}Al_{0.46}N$ look quite different and the latter spectrum resembles the TiN 200 one. The data treatment is focused on the Ti *K* pre-edge region, which is sensitive to the symmetry of the nearest neighbour's environment. A flat pre-edge peak is related to sixfold coordination of Ti atoms as in the f.c.c. lattice while a sharp pre-edge peak is assigned to fourfold coordination in the h.c.p. lattice with a stronger overlap of Ti 3*d* and N 2*p* empty electronic states. These analyses are supplemented with modelling of the pre-edge region using the *ab initio* full multiple-scattering code *FEFF9*.

As normalization of DAFS spectra recorded from different orientations of crystalline domains is difficult to carry out, a way to extract short-range-order information from the pre-edge region is presented. The energy-dependent smooth structure factor is calculated for each Bragg reflection of the analysed samples and adjusted to experimental spectra and then subtracted, for an easier comparison with XANES spectra of each sample. The examination of XRD and DANES data of cubic TiN and $Ti_{0.54}Al_{0.46}N$ film leads to the conclusion that the 111 domains of the latter present a better long- and short-range order than the 200 ones, assigned to the presence of more regular TiN_6 octahedra. In a well ordered lattice with few distortions the number of Ti atoms probably outweighs that of Al atoms. Thereby, the similar shape of $Ti_{0.54}Al_{0.46}N$ (111) and TiN (200) DANES suggests that more Ti atoms are incorporated in domains growing along the 111 direction than along the 200 one. In such complex materials, which present a competitive growth of domains with various orientations, the reduction of diffraction anomalous to pseudo X-ray absorption spectra could be a way to study short-range order within a crystallized area.

In conclusion, diffraction anomalous experiments performed in the region on two different growth orientations of PVD TiAlN thin films provide evidence of the difference in composition of 111 and 200 domains. Favouring the growth of Ti-enriched 111 domains in the deposition process should be an interesting way to improve mechanical properties of these hard coatings.

Acknowledgements

The authors would like to thank the staff of Synchrotron SOLEIL, and especially the DiffAbs beamline team for their support during the experiments and fruitful discussions. The experiments were supported by the synchrotron SOLEIL Community, which is greatly acknowledged. This work is partly supported by 'Pays de Montbéliard Agglomération'.

References

Adibi, F., Petrov, I., Greene, J. E., Hultman, L. & Sundgren, J. E. (1993). *J. Appl. Phys.* **73**, 8580–8589.
Adibi, F., Petrov, I., Hultmann, L., Wahlström, U., Shimizu, T., McIntyre, D., Greene, J. E. & Sungren, J. E. (1991). *J. Appl. Phys.* **69**, 6437–6450.
Alamagna, L., Prosperi, T. & Turchini, S. (1998). *J. Appl. Phys.* **83**, 3552–3555.
Ankudinov, A. L., Ravel, B., Rehr, J. J. & Conradson, S. D. (1997). *Phys. Rev. B*, **58**, 7565–7576.
Beckers, M., Schell, N., Martins, R. M. S., Mücklich, A. & Möller, W. (2005). *J. Vac. Sci. Technol. A*, **23**, 1384–1391.
Cromer, D. T. & Liberman, D. A. (1981). *Acta Cryst.* A**37**, 267–268.
Cross, J. O., Newville, M., Rehr, J. J., Sorensen, L. B., Bouldin, C. E., Watson, G., Gouder, T., Lander, G. H. & Bell, M. I. (1998). *Phys. Rev. B*, **58**, 11215–11225.
Ersen, O., Tuilier, M.-H., Gergaud, P., Thomas, O. & Lagarde, P. (2003). *Appl. Phys. Lett.* **82**, 3659–3661.
Ersen, O., Tuilier, M.-H., Keck-Thobor, A. & Rousselot, C. (2005). *Nucl. Instrum. Methods Phys. Res. B*, **234**, 308–320.
Farges, F., Brown, G. E. & Rehr, J. J. (1997). *Phys. Rev. B*, **56**, 1809–1819.
Gago, R., Redondo-Cubero, A., Endrino, J. L., Jiménez, I. & Shevchenko, N. (2009). *J. Appl. Phys.* **105**, 113521.
Hakansson, G., Sundgren, J. E., Mclntyre, D., Greene, J. E. & Münz, W. D. (1987). *Thin Solid Films*, **153**, 55–65.
Hodeau, J. L., Favre-Nicolin, V., Bos, S., Renevier, H., Lorenzo, E. & Berar, J. F. (2001). *Chem. Rev.* **101**, 1843–1867.
Hörling, A., Hultman, L., Odén, M., Sjölén, J. & Karlsson, L. (2005). *Surf. Coat. Technol.* **191**, 384–392.
Hugosson, H. W., Högberg, H., Algren, M., Rodmar, M. & Selinder, T. I. (2003). *J. Appl. Phys.* **93**, 4505–4511.
Jiang, N., Su, D. & Spence, J. C. H. (2007). *Phys. Rev. B*, **76**, 214117.
Jorissen, K. & Rehr, J. J. (2010). *Phys. Rev. B*, **81**, 245124.
Kawaguchi, T., Fukuda, K., Tokuda, K., Shimada, K., Ichitsubo, T., Oishi, M., Mizuki, J. & Matsubara, E. (2014). *J. Synchrotron Rad.* **21**, 1247–1251.
Kutschej, K., Mayrhofer, P. H., Kathrein, M., Polcik, P., Tessadri, R. & Mitterer, C. (2005). *Surf. Coat. Technol.* **200**, 2358–2365.
Mayrhofer, P. H., Hörling, A., Karlsson, L., Sjölén, J., Larsson, T., Mitterer, C. & Hultman, L. (2003). *Appl. Phys. Lett.* **83**, 2049–2051.
Musil, J. (2000). *Surf. Coat. Technol.* **125**, 322–330.
Padley, S. & Deevi, S. C. (2003). *Mater. Sci. Eng. A*, **342**, 58–79.
Pinot, Y., Pac, M.-J., Henry, P., Ulhaq-Bouillet, C., Ersen, O., Odarchenko, Ya. I., Ivanov, D. A., Rousselot, C. & Tuilier, M.-H. (2015). *Thin Solid Films*, **577**, 74–81.
Proietti, M. G., Renevier, H., Hodeau, J. L., Garcia, J., Bérar, J. F. & Wolfers, P. (1999). *Phys. Rev. B*, **59**, 5479–5492.
Rachbauer, R., Massl, S., Stergar, E., Holec, D., Kiener, D., Keckes, J., Patscheider, J., Stiefel, M., Leitner, H. & Mayrhofer, P. H. (2011). *J. Appl. Phys.* **110**, 023515.
Ravel, B. & Newville, M. (2005). *J. Synchrotron Rad.* **12**, 537–541.
Rehr, J. J., Kas, J. J., Prange, M. P., Sorini, A. P., Takimoto, Y. & Vila, F. (2009). *C. R. Phys.* **10**, 548–559.
Schalk, N., Mitterer, C., Keckes, J., Penoy, M. & Michotte, C. (2012). *Surf. Coat. Technol.* **209**, 190–196.
Stragier, H., Cross, J. O., Rehr, J. J., Sorensen, L. B., Bouldin, C. E. & Woicik, J. C. (1992). *Phys. Rev. Lett.* **69**, 3064–3067.

Tavares, C. J., Rebouta, L., Rivière, J. P., Girardeau, T., Goudeau, P., Alves, E. & Barradas, N. P. (2004). *Surf. Coat. Technol.* **187**, 393–398.
Tuilier, M.-H., Pac, M.-J., Anokhin, D. V., Ivanov, D. A., Rousselot, C. & Thiaudière, D. (2012). *Thin Solid Films*, **526**, 269–273.
Tuilier, M.-H., Pac, M.-J., Covarel, G., Rousselot, C. & Khouchaf, L. (2007). *Surf. Coat. Technol.* **201**, 4536–4541.
Tuilier, M.-H., Pac, M.-J., Gîrleanu, M., Covarel, G., Arnold, G., Louis, P., Rousselot, C. & Flank, A.-M. (2008). *J. Appl. Phys.* **103**, 083524.
Vedrinskii, R. V., Kraizman, V. L., Novakovich, A. A., Demekhin, Ph. V. & Urazhdin, S. V. (1998). *J. Phys. Condens. Matter*, **10**, 9561–9580.
Wahlström, U., Hultman, L., Sundgren, J.-E., Adibi, F., Petrov, I. & Greene, J. E. (1993). *Thin Solid Films*, **235**, 62–70.
Willmann, H., Beckers, M., Birch, J., Mayrhofer, P. H., Mitterer, C. & Hultman, L. (2008). *Thin Solid Films*, **517**, 598–602.
Woicik, J. C., Shirley, E. L., Hellberg, C. S., Andersen, K. E., Sambasivan, S., Fischer, D. A., Chapman, B. D., Stern, E. A., Ryan, P., Ederer, D. L. & Li, H. (2007). *Phys. Rev. B*, **75**, 140103.